Invited paper

OPTO-ELECTRONICS REVIEW **8**(1), 25–42 (2000)

The development of nitride-based UV photodetectors

D. WALKER and M. RAZEGHI*

Center for Quantum Devices, Department of Electrical and Computer Engineering
Northwestern University, Evanston, IL 60208, USA

In this review article, an analysis of the recent developments of nitride-based photodetectors is reported. At the beginning, a brief introduction sketches the background of GaN and AlGaN material properties and addresses issues concerning their application in existing systems. Next, the theory behind the operation of each device is discussed, followed by significant achievements in the processing technology and progress made in understanding how defects in the material affect the devices. Finally, the overall performance of photoconductors, p-n junction devices and Schottky barrier devices made from GaN and AlGaN is described in detail.

Keywords: nitride-based photodetectors, solar-blind p-n junction devices, high speed Schottky barrier devices.

1. Introduction

GaN, AlN and their alloys $Al_xGa_{1-x}N$ are promising materials for developing ultraviolet (UV)-visible optoelectronic devices because of their direct bandgaps and relatively high mobilities. By changing the Al-composition, x, from 0 to 1, the energy gap of this ternary material can be tuned from 3.4 eV to 6.2 eV, which spans the wavelengths from 365 nm to 200 nm. In particular, it includes the strategic window (240 nm to 280 nm) of ozone layer absorption. The intrinsic solar blindness of these detectors leads to many applications as illustrated in Fig. 1. Solar-blind UV photodetectors are critical components in many civilian and military applications including UV astronomy, flame sensors, early missile threat warning, chemical reagent detection, and secure space-to-space communications [1–3]. Solar blindness, which is the accurate detection of UV light in a strong visible and/or infrared background, requires an extremely high sensitivity of UV radiation relative to visible and infrared radiation. For example, objects studied in UV astronomy are often 4 to 8 orders of magnitude brighter in the visible than in the UV [2].

III-nitride materials, $Al_xGa_{1-x}N$ compounds, are the most suitable candidates especially for these airborne and space applications, which require the most lightweight and simple photodetector possible. Another consequence of their wide bandgap is intrinsic solar-blindness and low dark currents. III-nitride detectors would therefore not need Wood's filters or heavy cooling systems to eliminate longer wavelengths as silicon detectors do, thus reducing cost and launch weight [1,2]. Moreover, III-nitrides are both physically and chemically strong, which makes them ideal for radiation-intense space applications and less subject to aging.

*e-mail: razeghi@ece.nwu.edu

2. General theory

A certain understanding of the theory of photodetectors is assumed for this report. Due to the thorough handling of this subject in earlier books [4,5] and review papers [1] only a brief framework will be discussed here.

A general theory of photodetectors for a slab of homogeneous semiconductor material includes factors such as the spectral current responsivity, current noise, detectivity, and various noise mechanisms. The current responsivity depends on two main factors: the quantum efficiency, η, and the photoconductive gain, g, which are assumed to be constant over the volume of the device. The quantum efficiency is a measure of how well the input radiation is coupled to the electrical area of the photodetector. It is usually defined as the number of electron-hole pairs generated for each incident photon. When an electron or hole reaches the appropriate contact, and the excess carrier lifetime, τ, is greater than its transit time to the contact, t_r, another carrier will be injected from the opposite contact to maintain space charge equilibrium. Therefore, one photo-generated electron-hole pair can actually contribute to multiple carriers passing the contacts. The photoconductive gain is a measure of these resultant carriers and offers insight into how well the generated electron-hole pairs are used to generate the current of the photodetector. A simple equation for the photocurrent gain is $g = \tau/t_r$, and the spectral current responsivity is

$$\Re = \frac{\lambda\eta}{hc} qg \quad (A/W),$$

where λ is the wavelength of the incident light, h is Planck's constant, c is the speed of light, and q is the charge on the electron.

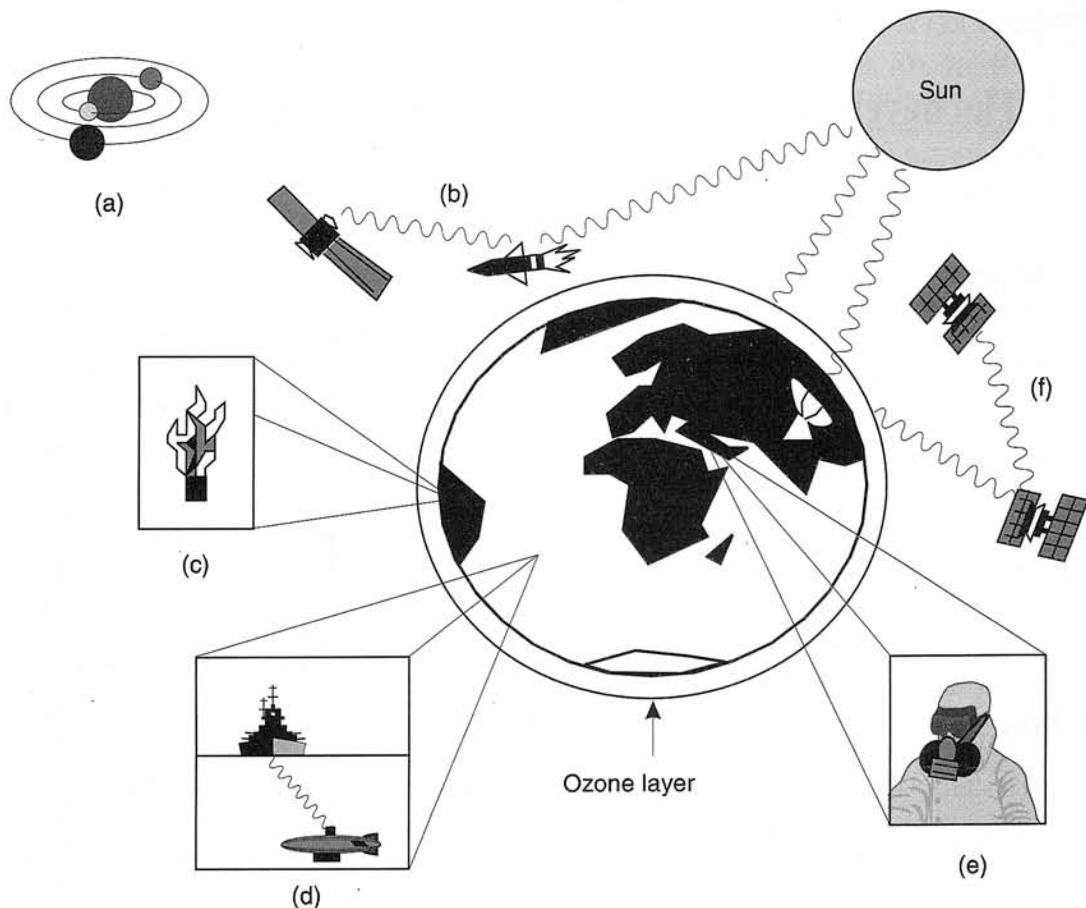

Fig. 1. Applications for UV photodetectors: (a) UV astronomy, (b) solar blind detectors, (c) flame detection and engine monitoring, (d) underwater UV communications, (e) chemical/biological battlefield reagent detector, (f) space communications secure from Earth.

Another important feature that photodetectors exhibit is the noise power spectral density S_n, which is usually 1/f limited, satisfying the relationship

$$S_n = S_0 \frac{I_d^2}{f^\gamma} \quad (A^2/Hz),$$

where I_d is the dark current, f is the frequency, and S_0 and γ are fitting parameters. The best fits are usually with $\gamma \sim 1$. The noise parameter S_0 should be independent of biasing. The total noise power generated in the photodetector is given as

$$P_n = \left\langle i_n^2 \right\rangle R_L \quad (W),$$

where R_L is the load resistance and i_n is the noise current. The total noise current representation is made up of 1/f noise, shot noise, and Johnson noise

$$\left\langle i_n^2 \right\rangle = \left\langle i_{1/f}^2 \right\rangle + \left\langle i_{shot}^2 \right\rangle + \left\langle i_J^2 \right\rangle.$$

The noise power is calculated as the area under the noise power spectral density curve in the bandwidth range, B. Hence for the 1/f noise contribution

$$\left\langle i_{1/f}^2 \right\rangle = \int_0^B S_n(f)\,df = \int_0^1 S_n(f)\,df + \int_1^B S_n(f)\,df$$
$$= S_0 I_d^2 + S_0 I_d^2 \int_1^B \frac{1}{f}\,df = S_0 I_d^2 (\ln B + 1),$$

although it is also common to just neglect the noise frequencies below 1 Hz and measure the area under the noise power spectral density graph directly. The 1/f noise dominates at low frequency.

The shot noise can be estimated by $\left\langle i_{shot}^2 \right\rangle = 2eI_d B$ [4,5], where e is the electron charge. This is also called generation-recombination noise because it describes the effects of generation and recombination centres created by the impurities or lattice defects in the material. The rates depend on the individual nature of the centre, its predominant state of charge carrier and the position of the level in the forbidden gap. Shot noise generally dominates at intermediate frequencies.

The spectral density of Johnson noise is constant--essentially white noise. It is associated with the finite resistance of the device, R, and is due to the random thermal motion of charge carriers in the semiconductor crystal, not to be confused with the fluctuation of the total number of

© 2000 COSiW SEP, Warsaw

charge carriers. The Johnson noise current can be written as

$$\left\langle i_J^2 \right\rangle = \frac{4kT}{R_{eq}},$$

where R_{eq} is the parallel combination of the junction resistance, the external load resistance and the input resistance of the amplifier. It is usually dominant at high frequencies due to the inversely proportional qualities of the other sources of noise to frequency. Because Johnson noise in inversely proportional to R, and the resistance of these wide band gap devices is usually very large, it follows that the Johnson noise does not play a large role in the noise behaviour.

The noise equivalent power (NEP) is commonly used to characterise photodetectors. The NEP is the incident light power necessary to obtain a unity signal to noise ratio in a photodetected signal, and is given by

$$NEP = \frac{\sqrt{\left\langle i_n^2 \right\rangle}}{\Re},$$

where $\Re$ is the responsivity of the photodetector, and i_n is the total noise current. Essentially, the NEP represents the minimum detectable signal.

The common figure of merit for many different types of photodetectors is the detectivity, D^*. It characterises the signal to noise performance of the device and is defined as

$$D^* = \frac{\Re\sqrt{A_{opt}B}}{\sqrt{\left\langle i_n^2 \right\rangle}} = \frac{\sqrt{A_{opt}}B}{NEP} \quad (cmHz^{1/2}/W),$$

where A_{opt} is the optical area of the detector. The normalised detectivity is a parameter used to compare different detectors.

Detectors are divided into two different categories: photoconductive and photovoltaic devices. Photoconductive devices do not have a built-in potential barrier. They operate by absorbing a photon with a greater energy, hν, than the band gap energy, E_g, which creates an electron-hole pair and changes the electrical conductivity of the semiconductor. The change in conductivity is measured by means of electrodes attached to the semiconductor surface and a biasing circuit consisting of a voltage supply and a load resistor. The signal is measured over the load resistor and is detected as either a change in voltage developed across the sample or as a change in current in the biasing circuit, depending on the relative resistance of the material.

In a photovoltaic detector a built-in field native to the semiconductor structure, rather than an external biasing circuit, separates the photo-generated charge carriers of opposite sign sending them, by way of drift current, to their respective metal contacts. Figure 2 demonstrates this with

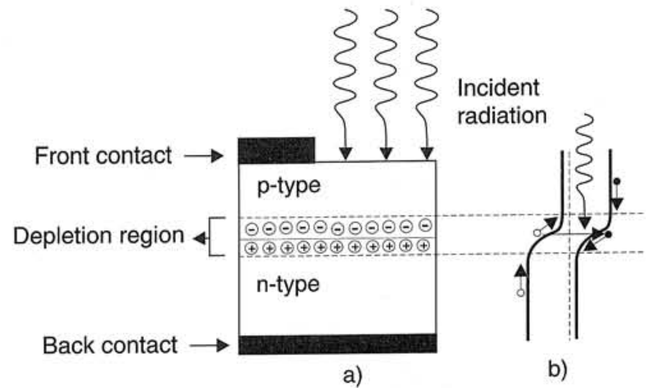

Fig. 2. Schematic and band diagram of a p-n junction.

a schematic and band diagram of the p-n junction. For high-speed operation the depletion region must be very thin to reduce the transit time of the carriers to the contacts. Alternately, employing a thicker depletion region, increases the quantum efficiency by escalating the fraction of incident light that is absorbed by the semiconductor crystal. Hence, there is a trade off between the detector's speed of response and the quantum efficiency. The device is said to be operated in a photovoltaic mode when it is unbiased and connected only to a load impedance, however in many cases a relatively large reverse bias is applied across the photodiode to reduce the carrier transit time and lower the device capacitance. The photovoltaic effect can be seen in many different structures such as p-n junctions, Schottky barrier diodes (metal-semiconductor diodes), and heterojunctions.

The three main types of photodetectors: photoconductors, p-n junction devices and Schottky barrier devices, are all considered useful for certain applications. In comparison, the photoconductors display the important advantage of internal photoelectric gain, which lessens the need for an amplifier, an additional source of noise to the system. The p-n junction, however, can be run at low or zero-bias currents, maintains a high impedance, and capability for high frequency operation at reverse bias. The Schottky diode is by far the easiest type of photovoltaic detector to fabricate. It also utilises a more efficient current transport process than p-n junction photodiode, which is limited by the diffusion process. A summary of this comparison between three different types of UV photodetectors is shown in Table 1.

3. Photodetector technology

This section discusses advancements made in the field of processing and fabrication technology for nitride based UV photodetectors. Although the processing of these photodetectors includes common techniques such as photolithography, metal evaporation and dielectric film deposition, the focus here will be on the facets of device construction that are uniquely difficult or challenging for nitride-based schemes, such as high quality ohmic/Schottky contacts and etching. These, normally routine, procedures become more difficult

Table 1. Comparison of different types of UV photodetectors.

Photodetector type	Advantages	Disadvantages	Challenges
Photoconductors	• Easy to fabricate • Internal photoelectric gain	• Low sped • Large dark current • Large Johnson noise	• Interdigitated patterns require enhanced resolution
P-n or p-i-n photodiodes	• Low or zero dark current • High-speed • High impedance (good for FPA readout circuitry) • Compatible with planar processing technology (for FPA) • For p-i-n photodiodes, easy optimisation of quantum efficiency and speed with i layer	• Speed is limited by minority carried diffusion time and storage time • Speed and quantum efficiency trade-off	• Etching is necessary to expose various layers • Ohmic contacts necessary to both n- and p-type material
Schottky photodiodes	• High efficiency • High speed • Easy to fabricate	• Require high absorption coefficient • No-sharp cut-off (below bandgap res.) • Front side illumination needed	• Schottky contact is needed

when working with a material system known for it's large band gap, physical hardness, and chemical inertness.

3.1. Electrical contacts

Both ohmic and Schottky contacts become challenging when faced with the large band gap of GaN, 3.4 eV. Ternary AlGaN material has an even higher bandgap, up to 6.2 eV (AlN), so the challenge of fabricating good Schottky contacts becomes greater. Low- -resistance ohmic and high quality Schottky contacts are a necessity for photodetector systems, so their study, characterisation and improvement are fundamental aspects of GaN-based UV detector development.

3.1.1. Low resistance ohmic contacts

Ohmic contacts to n-GaN

The earliest work in the investigation of ohmic contacts to GaN focused on the common materials used as contacts of other III-V semiconductor materials. Au and Al were tested [6] and the initial results indicated an agreement with the electronegativity correlation drawn up by Kurtin et al. [7]. This theory states that the dependence of the metal-semiconductor junction barrier height on the work function of the metal is related to the ionicity of semiconductor compound, as measured by the electronegativity difference. GaN, with an electronegativity difference of 1.87, lies in the area of the curve which indicates that the barrier height is directly dependent on the work function difference of GaN and the metal contact. Therefore, to attain a low barrier to current transport (ohmic contact) a metal must be chosen with a smaller work function than GaN. It is difficult to form an ohmic contact to GaN, with a measured work function of 4.1 eV, because there is no metal with a work function < 4.1 eV.

Even with annealing, the specific contact resistivities for Au and Al were on the order of 10^{-3}–10^{-4} $\Omega\,cm^2$ – too high for practical devices [6]. Later work utilized bilayer contacts, such as Ti/Au and Ti/Al, and demonstrated contact resistivities as low as 8×10^{-6} $\Omega\,cm^2$ [8]. These values were obtained by a rapid thermal annealing (RTA) of the contacts at 900°C for 30 seconds, which is believed to have led to a solid phase reaction at the interface of the Ti and GaN, creating TiN. This semi-metallic layer, coupled with residual nitrogen vacancies that caused the surface region to be n-doped [9], provided the configuration necessary for tunneling-based, ohmic contacts. The rapid thermal annealing of contacts to GaN soon became a popular method of obtaining low resistance ohmic contacts. This was later supplemented with a reactive ion etching (RIE) treatment of the semiconductor surface before metal evaporation to reduce the contact resisitivity further. Using Ti/Al/Ni/Au as the contact metal layers, Fan et al. [10] first exposed the GaN to a RIE, then deposited the metal layers, and lastly exposed them to RTA at 900°C for 30 seconds. This furnished the semiconductor-contact scheme with a specific contact resistivity of 8.9×10^{-8} $\Omega\,cm^2$ (although transfer length measurements are really only accurate down to 10^{-7} $\Omega\,cm^2$). The pre-metal deposition ion etching can result in ohmic contacts by removing the native oxide layer on the semiconductor surface, as well as forming a donor-like layer in the ion damaged region at the surface. The oxide removal proposition was confirmed by the fact that the difference in contact resistivities between a sample with RIE versus a sample without RIE persists even after the N_2 annealing treatment. If the benefit were from ion damage alone or from N sputtering of the surface then, presumably, the difference in resistivities would vanish after annealing, because the do-

 © 2000 COSiW SEP, Warsaw

nor-rich surface region of the RIE treated samples would either recover to its pre-etch status or be consumed in the TiN formation. Further mechanisms of ohmic contact realisation were suggested involving the metal layer themselves. It seems that a thick Al layer can prevent the diffusion of Ni and Au into the semiconductor at high temperatures, and the AuNi alloy formed over the AlTi layer is very robust and prevents the oxidation of Al, which would lead to an increase in the contact resisitivity [10].

As techniques for making contacts evolved the background doping of GaN became more easily controlled due to improved epitaxial techniques and purer precursors and carrier gasses. Also, doping with Si became known as an easy way to control the concentration of electrons in the layer. This led to a simpler approach for obtaining low resistance ohmic contacts to n-GaN employed by Gou et al. [11], involving the carrier concentration of the GaN contact layer. Ti/Ag contacts were evaporated on n-GaN samples with carrier concentrations ranging from 1.5×10^{17} to 6×10^{19} cm^{-3}. The specific contact resistivity was found to decrease with increasing carrier concentration giving a minimum resistivity of 6.5×10^{-6} $\Omega\,cm^2$ for a carrier concentration of 1.7×10^{19} cm^{-3} using no annealing or etching techniques. These types of contacts would be amenable on devices where growing a n^+ contact layer is easy and allowable, with the reward being the need for far fewer processing steps (i.e. RIE, RTA). But, whether these contacts would be suitable for use on devices exposed to high temperature remains to be seen. In the meantime, many different metals layer combinations such as Ag, Au, TiN, Au/Ti, Au/Mo/Ti, and Au/Si/Ti [12] were tested, usually with RTA processing, to investigate their thermal stability and ohmic characteristics. Ag and Au proved to be very unstable, poor ohmic contacts that diffused across the GaN surface at temperatures greater than 500°C.

The structure of the more popular contacts, Ti/Al and Ti/Al/Ni/Au, were studied by transmission electron microscopy (TEM), high-resolution electron spectroscopy (HREM), and electron diffraction [13]. Both HREM and electron diffraction established the presence of a textured polycrystalline layer of cubic TiN on the surface of the GaN, even before annealing. The thickness increased with annealing in both contact schemes. The GaN region near the surface contained many structural defects that could be nitrogen vacancies. Both schemes showed a dramatic decrease in resistivity after annealing. Two additional mechanisms were proposed for the reduction of contact resistivity by RIE:

- the surface roughness caused by the preferential etching of dislocated material creating an increased contact area,
- the radiation damage at the surface of the GaN aided in contact metal diffusion. Although the most important factor, by far, in obtaining low resistance ohmic contacts to GaN is the formation of TiN at the interface, which is believed to cause bending of the GaN conduction band sufficient for tunneling, additional types of low-resistance ohmic contacts should not be ignored. The other main form of this type of contact is the low barrier Schottky contact. Energy dispersive x-ray shows a certain amount of Al in the interfacial area (26.2 at. %), and a ternary Al-Ti-N compound might have a band gap close to that of GaN, hence providing the low-barrier Schottky contact necessary for low resistance [13].

Even more interest was taken in the Ti/Al contact scheme. X-ray photoelectron spectroscopy (XPS) depth profiles were performed by Luther et al. [14] to analyze the atomic percent of the metal alloy through its entire depth. Using this method they were able to determine that a low resistance ohmic contact can be realised by annealing Ti/Al contact at relatively low temperatures (400–600°C). This is due to the reduction of the native gallium oxide by the Ti and the formation of a low-work function intermetallic Ti-Al phase in contact with the GaN. The GaN showed no decomposition at all and the Ti-Al provided a low barrier, allowing current to flow in either direction. The resultant contact resistivity, 5×10^{-6} $\Omega\,cm^2$, was the lowest reported that did not use RIE or RTA techniques.

Lester et al. [15] were able to shift the focus away from a post evaporative annealing procedure briefly by demonstrating an ohmic contact with specific contact resistance as low as 1×10^{-5} $\Omega\,cm^2$ using a 1120°C implant activation anneal and Ti/Al contacts. This decrease in resistivity was possibly due to the desorption of nitrogen from the GaN at high temperatures leaving nitrogen vacancies (n^+–GaN) behind. A much lower contact resisitivity, 3.6×10^{-8} $\Omega\,cm^2$, was achieved by Burm et al. [16] using an activation anneal (1150°C, 30 s) of the implanted silicon and Ti/Au contacts. Though this method is very versatile, drawbacks of the implanted contacts include the high temperature anneal required to activate implanted donors, and the necessity of realignment for metal contact placement, not to mention the complexity of the implantation process itself.

After noticing the trend towards TiN formation at the contact interface, but aware of the shortcomings of Al (low melting point, easily oxidised) in contrast to the stable GaN, Wu et al. [17] developed a method without Al that still relied on the high temperature Ti anneal. This method involved the evaporation and subsequent annealing of Ti followed by the realignment and evaporation of Ti/Au and gave a specific contact resistivity of 3×10^{-6} $\Omega\,cm^2$. This removed the threat of Au diffusion into the GaN, although incorporated additional processing steps.

Other metal configurations including Nd [18] and Pd [19] have been attempted with post annealing techniques and have offered relatively low contact resistivities ($\sim1\times10^{-5}$ $\Omega\,cm^2$) at low temperatures (~600°C).

Ohmic contacts to p-GaN

Ohmic contacts to p-GaN have always posed more of a challenge to device development. The main obstacles to developing device quality ohmic contacts on p-type GaN

are the difficulties in growing heavily doped (> 10^{18} cm^{-3}) GaN and the absence of metals having work functions greater than that of p-GaN (~7.5 eV). These problems have hindered the quality of contacts, keeping the resistivity value ≥ 10^{-2} $\Omega\,cm^2$ for many different metal schemes [20]. A very thorough study by Ishikawa et al., using Pt, Ni, Pd, Au, Cu, Ti, Al, Ta, and Ni/Au as contact to p-GaN, analysed the effects of surface treatments of the p-GaN prior to metal evaporation as well as the contact resistivity dependence on metal work function [21]. Their results showed that GaO_x and adsorbed carbons on the surface of the GaN can be partially removed by a BHF treatment, and even more of this contamination layer can be removed by annealing the Ni and Ta contacts at ~500°C. These efforts to increase the abruptness of the junction did not significantly reduce the specific contact resistivity. The resistance decreased exponentially with increasing work functions, proving that the Schottky barrier height is sensitive to the work function of the metal. This reconfirms the choice of metals with high work functions for study as good ohmic contacts to p-GaN.

Very recently, work has been done using Pt/Ni/Au contact layers on p-GaN. The metal layers provide ohmic contacts with a resistivity of 3×10^{-3} $\Omega\,cm^2$ which can be lowered to 5.1×10^{-4} $\Omega\,cm^2$ after a 1 minute annealing at 350°C in a nitrogen atmosphere [22]. A more unique choice of metals was then utilised as Ta/Ti contacts were evaporated on moderately doped GaN:Mg samples [23]. These metals were chosen because they had enthalpies smaller then that necessary to form hydrides with Mg atoms, therefore they could possible facilitate the out-diffusion of H atoms from the GaN epilayer and increase the ionisation efficiency of the Mg atoms. With a ratio of 600 Å/400 Å the Ta/Ti layer provided a specific contact resistivity of 3.2×10^{-5} $\Omega\,cm^2$. Unfortunately, room temperature storage degradation is still a problem with this configuration. One contact to GaN:Mg that is very popular is Ni/Au, due to the high work function of Ni. Ho et al. [24] took advantage of another quality of Ni for their improved contact scheme. After evaporating Ni/Au layers in the surface they annealed the structure in air or oxygen between 300–600°C to intentionally oxidise the Ni. The specific contact resistivity decreases after the annealing (1×10^{-4} $\Omega\,cm^2$) and the transparency of the contacts improved to 65-80% for the range of 450-550 nm. The low resistance ohmic contact could be related to the formation of NiO which acts as a p-semiconductor (p ~1.3×10^{19} cm^{-3}).

3.1.2. Schottky contacts

Schottky contacts are a very important facet of certain photodetector constructs. It is important that they provide a good barrier to current flow and have low leakage. These measurement of these two quantities, barrier height and current leakage, provide a metric to compare different contact configurations. There are currently three popular methods for measurement of the Schottky barrier height.

The current-voltage (I-V) method for solving for the Schottky barrier height is based on the thermionic emission model. For thermionic emission and V > 3 kT/q, the diode equations are [25]

$$J = J_0 \exp\left(\frac{qV}{nkT}\right),$$

$$J_0 = A^* T^2 \exp\left(\frac{-\Phi_B}{kT}\right),$$

where J_0 is the saturation current density, q is the electron charge, k is the Boltzmann's constant, T is the temperature (in Kelvin), A* is the effective Richardson coefficient, n is the ideality constant, and Φ_B is the effective barrier height. First, the current density J_0 can be found by plotting ln J versus V. The value for J_0 can be found from the intercept on the vertical axis, where V = 0. Once J_0 is found, Φ_B can be solved, using a value for the Richardson coefficient from theory [26]

$$A^* = \frac{4\pi m^* qk^2}{h^3},$$

where $m^* = 0.20\ m_0$. It is not necessary to know A* very accurately, because an error of a factor of two gives rise to an error of less than kT/q in Φ_B. The barrier height found using this method is called the zero-bias barrier height, and is shown in Fig. 3(a). It includes the image force lowering

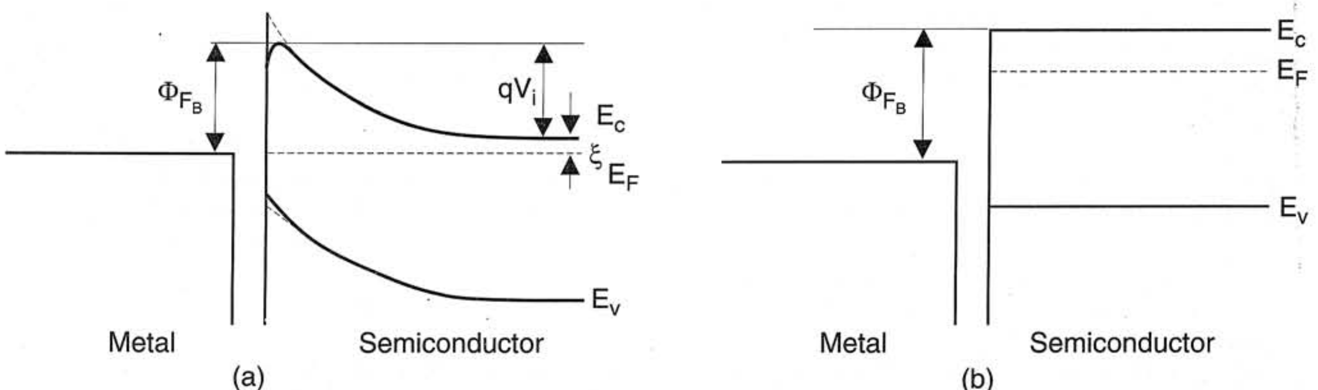

Fig. 3. (a) Zero-bias Schottky barrier height and (b) flat-band Schottky barrier height.

 © 2000 COSiW SEP, Warsaw

effect. The slope of the forward I-V characteristic also provides the ideality constant, which is a measure of how ideal the thermionic emission current transport is. This value should be close to unity (anything greater than 1.2 may be indicative of the presence of an interfacial layer) [27].

If A* is not known, the I-V characteristics can be measured over a range of temperatures and hence produce J_0 as a function of T. In this current-voltage-temperature (I-V-T) method, Φ_B and A* are measured from a fit of the plot $\ln(J_0/T^2)$ versus 1/T, based on the same equations as above. This plot will give a straight line with slope, $-q\Phi_B/k$, and an intercept on the vertical axis equal to ln(A*). Again, this refers to the zero-bias barrier height, although the surface preparation and thermal annealing of the diode may cause a slight difference between I-V and I-V-T values.

The capacitance-voltage (C-V) method for solving for the Schottky barrier height is rooted in the C-V relationship for a Schottky barrier, which is [5]

$$\frac{1}{C^2} = \frac{2}{qN_x A^2 \varepsilon_0 \varepsilon_s}\left(V_{bi} - V_a - \frac{kT}{q}\right),$$

for non-degenerate semiconductors, where C is the capacitance of the junction, N_x is the density of either donors (if n-type semiconductor) or acceptors (if p-type semiconductor), A is the junction area, ε_0 is the permittivity of free space, ε_s is the permittivity the of the semiconductor (dielectric constant), V_{bi} is the built-in voltage, and V_a is the applied voltage. The built in voltage can be written as $eV_{bi} = \Phi_{FB} - \xi$, where Φ_{FB} is the flat-band barrier height and ξ is the energy difference between the conduction band and the Fermi level in the steady state region of the energy bands. The flat-band Schottky barrier is described in Fig. 3(b). A plot of $1/C^2$ versus reverse bias should give a straight line with slope proportional to the carrier concentration, and horizontal axis intercept equal to ($\Phi_{FB} - \xi - kT/q$). This method does not include the image-force lowering effect.

The flat-band barrier height is essentially the measurement of the Schottky barrier height without an electric field present in the semiconductor (i.e., a sufficient bias was applied to the system to make the depletion region disappear). This flat-band measurement is important for actual junction measurements where an interfacial region might be present. If there is no interfacial layer, the barrier height is independent of any electric field which may exist inside the semiconductor. However, when there is an interfacial layer present, an electric field in the semiconductor changes the potential across the layer and modifies the barrier height. With an electric field present, the barrier height is reduced from the flat-band value by an amount which is proportional to the maximum electric field in the semiconductor and the thickness of the interfacial layer [25]. The zero-bias barrier height, found by I-V and I-V-T methods, is reliable only if the forward plot of ln J versus V is a straight line with $n < 1.1$. Any larger n value or non-linear plot is indicative of a thick interfacial layer, in which case the barrier height can not be clearly defined by the zero-bias measurement. Researchers get a variety of values for measured barrier heights, depending on the method of measurement. Care must be taken to make sure that the most accurate method is used.

Schottky contacts to n-GaN

Many groups have catalogued the barrier heights and ideality constants after having evaporated various metals onto cleaned semiconductor surfaces [28–32]. There is not the plethora of pre-treatment options that are used for the technology behind ohmic contact to GaN (acid rinse, RIE, annealing, etc.), but the GaN layers are commonly degreased, dipped in BHF, and rinsed in de-ionised water before processing the contact layers. From the research performed on ohmic contacts to GaN, a certain barrier height dependence on metal work function, Φ_m, has been demonstrated [21]. Therefore a logical choice for a good Schottky contact to n-GaN involves a metal with a high work function. Several methods, such as current-voltage (I-V), capacitance-voltage (C-V), temperature-dependent I-V (I-V-T), and internal photoemission, exist to measure the barrier height. The barrier heights for some metals with a high work function are listed in Table 2.

In some cases, a bilayer contact was found to be more thermally stable than its single layer counterpart, such as PtSi versus Pt on n-GaN, but the alloy did not have as high a Schottky barrier, Φ_{Bn}(PtSi) = 0.74 eV [33]. Other times, the Schottky barrier height is found to increase with subsequent annealing as was seen with indium tin oxide (ITO) on n-GaN [34]. The barrier monotonically rose from 0.68 eV to 0.95 eV with annealing up to 600°C for 15 minutes. The increase in barrier height may be due to the formation of an interfacial layer at the interface. Care must be taken when annealing contacts, especially Ni and Ni/Au on GaN, at high temperatures (> 700°C) as it leads to metal island formation and non-uniform metal penetration [35].

Schottky contacts to p-GaN

A systematic study was carried out concerning the Schottky barrier height at the interface of the common contact metals to p-GaN [20]. The Schottky barrier heights were obtained for Pt (Φ_{Pt} = 5.65 eV), Ni (Φ_{Ni} = 5.15 eV), Au (Φ_{Au} = 5.10 eV), and Ti (Φ_{Ti} = 4.33 eV) on p-GaN from the I-V characteristics. Although the resistivities were too high for device use, there was a correlation drawn. As the work function decreased, the barrier height increased slightly. This dependence was weak, therefore the metal work function was not the dominant factor affecting the Schottky barrier heights. Other causes could have been the interfacial states at the surface of the semiconductor as well as damage to the layer. Although the p- and n-type Schottky barrier heights should sum approximately to the band gap of the GaN, these metal/p-GaN barrier height val-

Table 2. The barrier heights of some common high work function metals to moderately doped n-GaN.

	Barrier heights ($q\Phi_m$)						
Meas. technique	Pt (5.65 eV)	Pd (5.12 eV)	Cr (4.50 eV)	Au (5.10 eV)	Ni (5.15 eV)	Ag (4.26 eV)	Pb (4.25 eV)
I-V	1.13 eV	1.11 eV	0.53 eV	1.03 eV	1.15 eV	0.82	0.73
C-V	1.27 eV	1.24 eV	0.58 eV	1.03 eV	1.11 eV		
I-V-T	1.03 eV	0.96 eV					
	Refs. 28,30		Ref. 31			Ref. 32	

ues were much too small (only 0.5-0.6 eV). Recently, Shiojima et al. [36] has demonstrated a large Schottky barrier on low Mg doped p-GaN. A preliminary study indicated that the surface of p-GaN became rougher as the Mg doping increased. Rough surfaces have been known to lead to leaky I-V characteristics for Ni Schottky contacts on n-GaN [37]. Without this leaky behavior the true barrier height was measured by I-V methods as 2.4 eV. This was in good agreement with the prediction that the sum of $q\Phi_B$ of n- and p-types add up to the band gap.

Besides being important for the fabrication of Schottky barrier photodetectors, the investigation of the barriers that arise between metal and semiconductor can help to further the understanding of ohmic contacts. One such popular metal choice for ohmic contact on n-GaN is Ti. Studies have been done analysing the barrier in this contact scheme with respect to low-temperature annealing [38]. The effective barrier height, measured by I-V-T, is initially ~200 meV, but increases to 250 meV after annealing at 60°C, and stabilises at 450 meV for annealing at 230°C and above. Rutherford backscattering and x-ray diffraction experiments indicated no macroscopic interfacial region between the Ti and GaN film after such annealing. The changes must, therefore, have been on a microscopic scale, such as the consumption of a few monolayers of oxide, which lead to a more intimate metal-semiconductor contact.

3.2. Etching

GaN and its related alloys are well known for the physical properties that make them so resilient to harsh conditions and applicable for use in hazardous environments. These benefits turn into obstacles when speaking of the processing and fabrication of devices based on this material system. This is because many devices require a multi-layer format, such as the p-n junction photodiode, where the material must be etched down to the n-GaN layer for the placement of a contact. This is not a trivial achievement considering the strength and chemical inertness of the material. Wet chemical etching is a very popular technique that is often used for this purpose in other III-V semiconductor systems. KOH has been found to etch AlN, but does not affect GaN similarly [39]. And while recent work with photoenhanced wet chemical etching has produced favorable etch rates in n-GaN [40], the technology is still not developed for p-GaN, which is frequently the top layer in a GaN device structure and, hence, most commonly etched. Therefore, methods involving reactive ion etching have been investigated and found to be a reasonable solution to the challenge of etching nitride-based materials. Although reactive ion etching has succeeded were other methods have failed, it also offers benefits that other etch methods, such as wet etching and sputtering, cannot. In reactive ion etching there is a synergistic relationship between the chemical reaction which takes place on the surface of the material and the removal of the reactants from the surface. A fresh surface is exposed by the bombarding ions which aids the chemical portion of the etching. The ion bombardment also serves to maintain directionality, stimulate the chemical reaction on the surface and help to desorb the product species. More elaborate additions to the basic RIE system, such as electron cyclotron resonance (ECR) and inductively coupled plasma (ICP), are used to couple a higher energy into the plasma, thereby increasing the density of ions by about two orders of magnitude [41]. This increases the etch rate, but does not increase the amount of damage incurred by the semiconductor, because only the ion density- not the ion energy- is increased. Recently, chemical assisted ion beam evaporation (CAIBE), which has been shown to be successful in highly controlled (directional) etching of GaN, has been reported for the etching of GaN laser facets [42]. RIE, ECR [43,44] and ICP [45,46] techniques remain the most popular for nitride detector fabrication.

Many different masks have also been investigated for the pattern transfer of devices into the GaN material, as well as different plasma chemistries, process pressures and temperatures, ion energy levels and ion density levels. Vartuli et al. [47,48] has reasoned that the limiting step in the etching of nitride-based compounds compared to other III-V material is the initial breaking of bonds at the surface, due to the higher bond energies for nitride based compounds. This means that strict control of the ion energy, and a high density of ions is necessary to etch GaN effectively. Most research has focused on achieving a reasonable etch rate while maintaining a smooth, anisotropic, controlled etch. There are many obvious things that affect the etch rate, such as the chemistry of the plasma. Among the others are: rf power (which affects the dc bias), process pressure, microwave power (ECR) or ICP power, electrode

 © 2000 COSiW SEP, Warsaw

temperature, material quality, and percent of active chemical species in the discharge. The most popular etch recipes are based on chloride (Cl_2, $SiCl_4$, BCl_3) or fluoride (SF_6, CF_4) chemical species, and provide etch rates from 10^3–10^4 Å/min.

Low damage etching is necessary to fabricate photodetector mesas without providing leakage current paths down the etched walls of the mesa. The etching process should be matched with an appropriate mask to ensure reliability and high selectivity of etching. Common etch masks are photoresist, metal, and dielectrics such as SiO_2 and Si_3N_4.

4. Defect effects in nitride photodetectors

Abnormally high responsivities and persistent photoconductivity (PPC) with long response times characterise many photoconductors made from nitride-based materials. PPC is photoinduced conductivity that persists after the termination of the photoexcitation. Several groups have also observed a frequency dependence of the photosignal and its non-linearity with incident power [62,64]. Much of the early work on PPC focused on comparisons of the nature of this decay to that caused by the DX centres in AlGaAs [49], which have identical decay kinetics. This connection led researchers to the stretched exponential function as a model for PPC decay in GaN

$$I_{PPC} = I_{PPC}(0)\exp\left[-\left(\frac{t}{\tau}\right)^{\beta}\right], \quad (\beta < 1)$$

where $I_{PPC}(0)$ is the maximum PPC buildup level, at the moment the excitation is removed, t is time, τ is the PPC decay time constant, and β is the decay exponent. The latice relaxation models for the AX centres describe the temperature dependence of τ

$$\tau \propto \exp\left(\frac{E_c}{kT}\right),$$

where E_c is the capture barrier.

Mg doping in GaN structures is not well understood, and improvements of the doping efficiency and quality are necessary to obtain p-type conduction lacking unstable impurities that affect conduction mechanics. Johnson et al. [50] first investigated PPC in GaN:Mg layers, grown by MOCVD. The thermal activation energy of the activated Mg acceptor was measured to be 131 meV. After analysing the dark current as a function of time for different temperatures, it was concluded that there are most likely two different states of neutral impurities in p-GaN. One is a metastable state (entered into immediately after capturing a hole), and the other a stable state, with a potential barrier existing between them in both the dark and photoexcited state. Although this group recognised the connection to the behaviour of DX centres in AlGaAs, the results were inconclusive due to the possibility that the behaviour was associated with the presence of isolated H impurities or Mg-H complexes in the lattice. Therefore, this group continued the investigation of GaN:Mg, grown by MBE (H free) as well as MOCVD (H rich) [51]. Using the stretched exponential function to define the PPC kinetics, an energy barrier of about 129 meV was found in the H-free GaN. This barrier prevents free hole capture by ionised Mg impurities. Lattice relaxation associated with Mg impurities was confirmed. The PPC effects were much larger in the MBE grown GaN, although the dark conductivity was in equilibrium, and did not need time to stabilise, as in MOCVD grown samples.

Binet et al. [52] investigated the long response times in n-GaN, grown by MOCVD. They used the kinetics of the photoresponse to demonstrate the existence of deep levels in the band gap acting as recombination centres, as evidenced by their weak temperature dependence. Two competing processes, bimolecular recombination (hyperbolic) dominating at high optical power range, and monomolecular recombination (exponential) involving long response times, were revealed.

The investigation of PPC effects in n-GaN as well as undoped GaN was linked to yellow luminescence in a report by Chen et al. [53] Both the photoluminescence and photoconductivity spectra showed a broad yellow band centred around 2.2 eV. The PPC effect could be observed for subband photon energies only down to 2.2 eV, thus implying that the PPC effects and the yellow luminescence arise from the same intrinsic defect. This defect was assumed to be intrinsic because the PPC effect was observed in undoped, Mg-doped, Se-doped and Si-doped GaN layers, but not in any layers that lacked yellow luminescence. The stretched exponential function and temperature dependence mentioned above aptly described the decay kinetics. The most probable candidate for the intrinsic defect responsible for the yellow luminescence, and possibly the PPC effects, was proposed to be a nitrogen antisite, N_{Ga}, in the GaN film. Later work by Reddy, et al. [54] strengthened the claim that PPC and yellow luminescence are related to each other.

Hirsch *et al.* [55] reported the observation of metastable behaviour, which manifested itself as PPC, in high-quality, unintentionally doped n-type GaN. They estimate an optical ionisation energy of 2.7 eV, which was large compared to the mean capture barrier of 0.2 eV. This capture barrier was slightly higher than previous reports [51]. PPC was also observed at room temperature for Si-doped n-GaN films grown by MOVCD [56]. Analysed in the context of stretched exponential parameters, Hall data and photoluminescence data, the cause of the PPC was found to be the same among samples with different mobilities, growth conditions, and thickness. Additionally, the growth of a sample lacking PPC phenomenon demonstrated the possibility for such high quality growth.

Qiu and Pankove [57], using MOCVD-grown p-type and unintentionally doped n-type GaN, attributed the PPC

in p-GaN to metastable centres at 1.1, 1.40, and 2.04 eV above the valence band edge. It was also argued that Ga vacancy is the candidate for PPC effects in n-type GaN. This is because the Ga vacancy can easily act as a hole trap and once the charge state changes, structural relaxation is expected.

AlGaN/GaN heterostructures were analysed for the presence of PPC by two separate groups. One observed a broad distribution of defect levels within the band gap [58], and that other correlated observed PC transient characteristics with the effects of PPC [59].

5. Photoconductors

The initial developments of GaN-based photoconductive detectors have been covered in an earlier review [1] therefore the early work will only be briefly outlined here. The first photoconductors utilising GaN were fabricated by Khan *et al.* [60]. The 0.8 μm thick, semi-insulating GaN was grown by MOCVD and, when contacted with 5000 Å thick Au contacts and illuminated, gave a responsivity of 2000 A/W at 365 nm. The visible rejection, the ratio of ultraviolet light to visible light detected, was $\sim 10^3$, with a linear photosignal over five orders of magnitude of input power. Initially the detectors fabricated using MBE grown GaN did not supply such a high gain as the MOCVD grown device, offering a current responsivity of only 125 A/W at 254 nm [61]. MBE was also used to grow GaN on Si (111) substrates, resulting in very low responsivity, 12 A/W at 4 V/340 nm [62]. The photocurrent was linear only for low power, and the saturation of the responsivity implied that carriers, probably holes, were being captured at either Mg deep acceptor sites or Mg-related traps or recombination centres, leading to a prolonged carrier lifetime.

Inevitably, fabrication of photoconductors began solely for the purpose of studying defect states in the GaN films [63]. The kinetics of photoconductivity in MOCVD-grown GaN films were elucidated by Kung et al. [64] who observed sub-linear response and excitation dependent response times at low excitation levels. This led to the conclusion that there was a redistribution of charge carriers with increased excitation level, which had the impact of decreasing the photoconductive gain with increasing UV intensity. The investigation of kinetics was continued by Binet et al. [65] who studied the steady-state and transient response of non-intentionally doped, MOCVD-grown GaN photoconductor. This detector had a responsivity of 4000 A/W at low power density with a large tail beyond the cutoff wavelength, indicative of deep levels distributed through the wide energy gap. The decrease in responsivity at higher power was due to intrinsic recombination, and not traps, because the process was only weakly dependent on temperature. At low power the photoresponse decay was exponential ($\tau = 3.9$ ms) consistent with mono-molecular recombination, and at high power (> 40 W/m^2) the photoresponse decay hyperbolic ($\tau = 2.6$ ms), which is consistent with bi-molecular recombination. Based on their model, the limiting factor was the electron capture time (on the order of milliseconds).

A very important use of the nitride-based detectors involves the solar blind capabilities of the ternary AlGaN material. By changing the Al composition the cutoff wavelength of AlGaN photodetectors can cover the spectrum from 200 to 365 nm at room temperature. In particular, it includes the strategic window (230-280 nm) of ozone layer absorption. It had been difficult to obtain high-quality AlGaN material with high Al content due to problems with growth technology. Using MOCVD growth techniques, Walker *et al.* [66] were able to demonstrate efficient $Al_xGa_{1-x}N$ photoconductors ($0 < x < 0.50$), with a minimum wavelength cutoff of 260 nm, well within the window for ozone absorption and pure solar blindness. These detectors were limited by a short carrier lifetime caused by the high Al content. After this first announcement, this same group achieved results on $Al_xGa_{1-x}N$ photoconductors ($0 < x < 1$), demonstrating the entire ternary scale [67]. The detectivity decreased with increasing Al composition, and one proposed mechanism to describe the increasing carrier lifetimes was the appearance of a trapping layer as the Al concentration is increased. Muńoz *et al.* [68] offered a unique photoconductor gain mechanism to explain their photoconductor results on MBE and MOVPE-grown, unintentionally doped GaN on Si (111). Similar to previous cases mentioned, the gain decreased with increasing power. The high sensitivity, non-linear response with power and non-exponential recovery were all be explained by modulation of the conductive volume of the layer.

6. Photovoltaic detectors

6.1. P-n junction photodiodes

The first photovoltaic effects in a GaN p-n junction structure were reported by Zhang *et al.* [69], who estimated the diffusion length of holes in the n-type GaN region to be 0.1 μm by modeling the spectral response shape. It is interesting to note that this work was undertaken without mature etching techniques for GaN material, which necessitated a novel contact configuration scheme for the n-GaN contact. Confirmation of the 0.1 μm hole diffusion length using a numerical model was later provided by Binet *et al.* [70]. Later work was performed comparing GaN p-n junction structures with 0.5 μm p-GaN/1 μm n-GaN structure versus a 0.5 μm n-GaN/1 μm p-GaN structure grown by MOCVD on sapphire [71]. Each detector was front-side illuminated furnishing a peak responsivity of 0.09 A/W at 360 nm, comparable to a UV enhanced Si p-n detector. The rise and fall times of these detectors were still slow though, on the order of 0.3 ms.

The first GaN p-i-n junction detectors grown by MBE demonstrated improvements in both the sensitivity and response speed compared to their MOCVD p-n junction counterparts. The structure consisted of a 1 μm thick n^+

 © 2000 COSiW SEP, Warsaw

layer, followed by an undoped GaN layer and capped by a 3000 Å thick p-GaN [72]. The responsivity value at 360 nm was 0.11 A/W, corresponding to a 48% internal quantum efficiency, and the visible rejection was ~10^3. The reverse bias leakage was 50–170 μA/mm^2 at 3 V reverse bias, and was attributed primarily to surface damage by the RIE etching of the mesas. The response time of the diodes was improved to 8.2 μs, and although excellent linearity of the photoresponse was observed, it was only tested at low power levels (< 0.9 W/m^2). Soon after, another realisation of p-i-n detectors using MBE grown material was reported by Xu et al. [73]. Using an AlN buffer layer, 3 μm thick n-GaN layer, 1 μm thick undoped GaN layer, and either a p-GaN layer (thickness ranging from 0–0.2 μm) or a 0.2 μm thick p-$Al_{0.12}Ga_{0.88}N$, they compared front side illuminated p-i-n detectors. In an investigation of the optical penetration depth of incident optical power and carrier diffusion in the p-GaN material, it was noted that as the p-GaN thickness was decreased the responsivity of the detector increased, up to 0.07 A/W at 364 nm. The zero bias response time for the detector was 29 ns. The responsivity was increased even further, 0.12 A/W at 364 nm, when the p-AlGaN layer was employed. The larger band gap of the ternary material allowed all of the light with energy less than 3.7 eV to pass through and be absorbed in the depleted intrinsic region. The visible rejection was about 10^3, and the response time of the detector was 12 ns at zero bias. The noise equivalent power (NEP) for the homojunction p-i-n and heterojunction p-i-n was 4 and 8.3 pW/Hz$^{1/2}$, respectively.

With the responsivity values of the GaN-based photodetectors now meeting the specifications set by UV-enhanced silicon and SiC detectors, the leakage current, noise, and speed became the focus of further improvement. Osinsky et al. [74] reported a GaN p-π-n detector grown by MOCVD that had a zero bias responsivity of 0.1 A/W (at 363 nm) and a dark current of 67.5 pA/mm^2 (at –3 V). The time response of 17.4 ns was RC time limited and the NEP was only 6.6 fW/Hz$^{1/2}$. Upon further investigation it was noted that the dark current scaled with the area of the device, indicating that the leakage path was through the volume of the device rather than the surface states as noted previously [72] in the MBE grown p-i-n photodiode. It was concluded that the main physical mechanism responsible for the leakage current was field dependent tunneling (hopping) over defects, such as grain boundaries and dislocations, in GaN. The 1/f noise observed was then explained by the fluctuating occupancy of these trap states. Seizing the opportunity to study the role of dislocations in GaN p-n junction detectors, Kozodoy et al. [75] compared the leakage currents of two different p-n junction photodiodes on laterally overgrown GaN. One set of p-n junction devices were positioned over the window area, where the growth from the substrate was purely vertical and dislocations seeded at the buffer layer could propagate upward. The others were placed over the laterally grown GaN, which was virtually free of vertical threading dislocations. Results showed that the dark current dropped from 9 mA/μm^2 for the first device placement, to 9 nA/μm^2 for a device over the low-defect area, an improvement in three orders of magnitude. Although deep trap levels still limited the device performance, this study confirmed the role that dislocations play in the noise level of GaN photodiodes. A report on GaN p-i-n detectors, by Walker et al. [76] demonstrated improvements in the responsivity (0.15 A/W) and rejection of visible light (10^6). The resistivity was demonstrated to be constant over five decades of optical power, as seen in Fig. 4. The large visible cutoff and constant responsivity over a wide range of power levels make this type of detector attractive for many applications.

Using heterojunction technology similar to the MBE-grown structure mentioned earlier, Krishnankutty et al. [77] fabricated p-i-n photodetectors, by MOCVD, which consisted of a sapphire substrate, AlN buffer layer, 1 μm thick n-$Al_{0.1}Ga_{0.9}N$, 0.25 μm thick undoped GaN layer, capped by a 1 μm thick p-GaN layer, as seen in Fig. 5(a). This back-side illuminated device gave a spectral response, shown in Fig. 5(b), with both a low and high wavelength cutoff, corresponding to the AlGaN absorption and the GaN low energy (< 3.4 eV) cutoff. The peak response in the UV band from 352–362 nm was ~0.2 A/W, corresponding to a quantum efficiency of 80%, and was nearly independent of the device area. The rejection is 10^2–10^3 on both sides of the active band with a slightly higher cutoff in the visible region. The leakage current was 30–75 pA/mm^2 (at < 10 V reverse bias).

It is indisputable that more research effort and energy have been invested in the p-i-n structure due to its versatility and theoretical effectiveness, but good results are nevertheless achievable with simple GaN p-n junction detectors as evidenced by the work of Monroy et al. [78]. Their front-illuminated device consisted of a 0.5 μm p-GaN layer and 1.4 μm n-GaN on a 1.6 μm unintentionally doped GaN layer, all grown by MOCVD. The responsivity was 0.145 A/W at 360 nm with a time response of 105 ns, limited by the RC time constant. These detectors also demonstrated a linear photocurrent for over five decades of incident optical power, up to 2000 W/m^2.

While heterojunction p-i-n structures can be employed to offer higher responsivities and band pass responses, only the incorporation of AlGaN in the active region can shift the response of the detector to lower wavelengths, which is imperative for solar blind applications. If the intrinsic region of a p-i-n structure consists of an $Al_xGa_{1-x}N$ layer then the p-layer (if front-side illuminated) must also have a larger energy gap ($Al_yGa_{1-y}N$ where $y \geq x$) or the input signal will be absorbed too close to the surface. The largest obstacle to achieving this goal has been a lack of the necessary doping capabilities for the p-AlGaN layer. The first demonstration of $Al_xGa_{1-x}N$ ($0 < x < 0.15$) p-i-n homojunction photodiodes was reported by Monroy, et al. [79]. The responsivity of these diodes ranged from 0.1 A/W to 0.01 A/W as the Al composition was increased to 15%. The visible rejection was on the order of 10^6, and the time re-

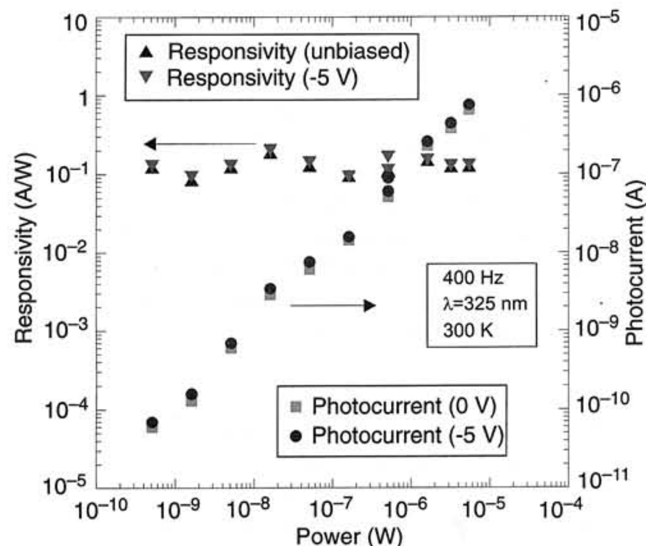

Fig. 4. Responsivity and photocurrent measured with increasing optical power (after Ref. 76).

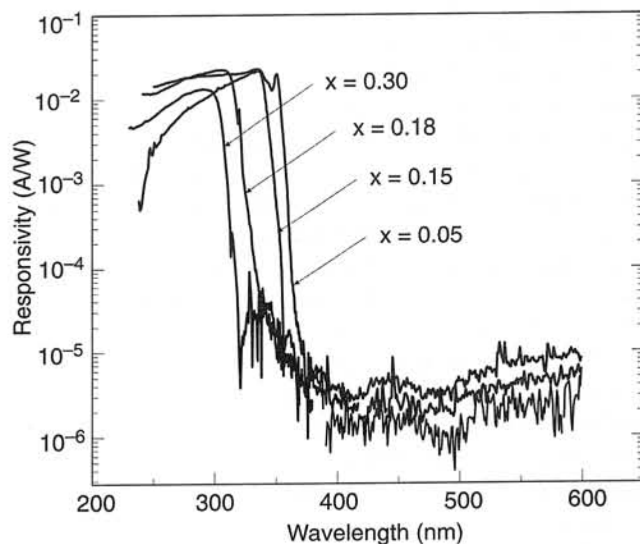

Fig. 6. Zero-bias spectral response of the $Al_xGa_{1-x}N$ p-i-n photodiodes (after Ref. 81).

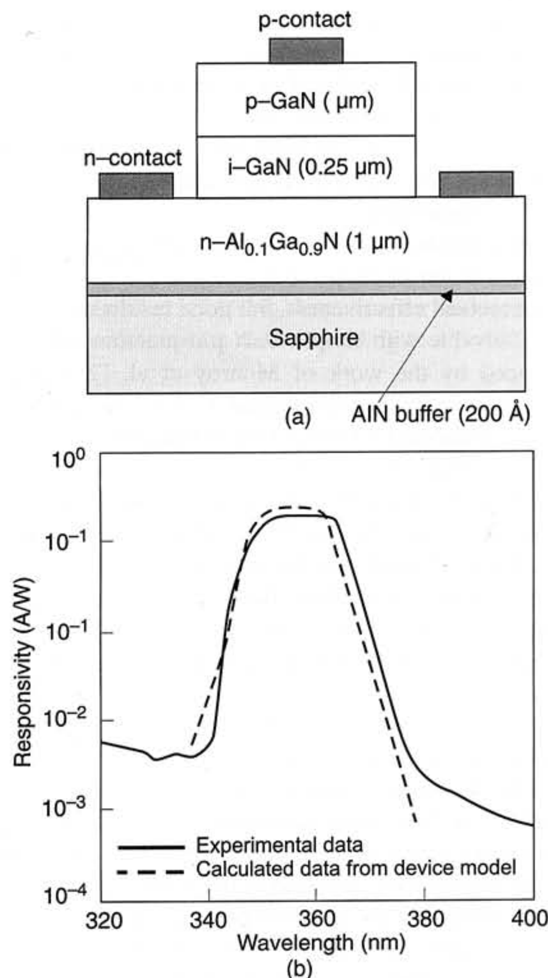

Fig. 5. Typical $GaN/Al_{0.1}Ga_{0.9}N$ heterojunction photodiode structure (a), and measured and calibrated spectral responsivity of typical $GaN/Al_{0.1}Ga_{0.9}N$ p-i-n photodiode on a logarithmic scale (b) (after Ref. 77).

sponse, which was not RC time dependent, was found to be ~500 ns. The device capacitance had strong frequency dependence and, after performing admittance spectroscopy measurements [27], an activation energy of 99 eV was calculated. This impurity was not related to deep levels, but possibly to substitutional Mg not completely activated at room temperature. These detectors had wavelength cutoffs as low as 338 nm, however the large amount of interest lies in the solar-blind region, which is below 270 nm [80]. This same group continued its investigation into AlGaN p-i-n detectors, increasing the Al concentration to 30% [81]. Although the responsivity remained low for high Al content devices (~0.02 A/W), and the time response increased with the Al incorporation, up to 0.9 μs, the cutoff wavelength was successfully shifted down to 291 nm, as seen in Fig. 6. Improvements need to be made in the areas of time response and responsivity, as there seems to be deleterious effects coinciding with the large Al concentration in the ternary material. Part of this problem might lie in the difficulties of p-doping the AlGaN layer, as well as obtaining a low resistance ohmic contact to it.

6.2. Schottky barrier photodiodes

Detectors based on Schottky barrier detectors are known for their high speed, efficiency and ease of fabrication. They are planar devices, so they do not require etching, nor do they even need a p-type layer. Requirements of a good Schottky barrier detector include a high-quality Schottky and low-resistance ohmic contact. Sometimes heterostructures, and subsequent mesa etching, are employed to acquire the necessary contact parameters. Many spectroscopic and flame sensing applications desire these types of detectors because of their zero-bias operation and sharp visible cutoff.

 © 2000 COSiW SEP, Warsaw

The first photovoltaic GaN detector was a Schottky barrier photodiode on p-GaN, reported by Khan et al. [82]. Using bilayer metals, Ti/Au and Cr/Au, for the Schottky and ohmic contact, respectively, a responsivity of 0.13 A/W at 320 nm was observed. The peak responsivity for this back-side illuminated detector occurred at 365 nm, with a drop of ~10^2 in the response from UV light to visible light. The device turned on at 1.5 V forward bias and experienced breakdown at 3 V reverse bias.

To avoid low quantum efficiency caused by the transmission of light through the highly-absorbing, defect-filled GaN-sapphire interface region, Chen et al. [83] employed front-side illumination on a GaN Schottky barrier detector. Other resourceful ideas were incorporated into the fabrication of this device, such as a transparent (70%) Schottky contact to achieve the maximum active area and minimum diffusion time of carriers to the contact, and a heterostructure design of n^--GaN on n^+-GaN, to optimise the contact properties. The structure of this device is shown in Fig. 7(a). The noise characteristics of the diode were also reported. The turn-on voltage was 0.8 V, with a barrier, measured by I-V-T methods, in good agreement with the value reported for the Schottky barrier height of thick Pd contacts on GaN [29]. The reverse bias breakdown was at –20V. The total quantum efficiency, benefiting from the device design, was greater than 65%, giving a peak current responsivity value of 0.18 A/W, as seen in Fig. 7(b). The RC-limited response speed of the device was 54 ns (fall time 118 ns), and the dark current was 5 nA/mm^2 at –5V. The detector was 1/f noise limited with a NEP of less than 4×10^{-9} W, which is in the same range as established Si-based commercial photodiode detectors.

This same group then tailored the band edge, as reported by Osinsky et al. [84], fabricating Schottky barrier detectors from $Al_xGa_{1-x}N$ (x = 0.26), thus demonstrating wavelength cutoffs at 290 nm. The Schottky contact metal was Pd, the ohmic contact metal structure was Ti/Au/Ti/Au, and the same dual layer n^-/n^+ scheme was utilised. The device turn-on voltage increased to 1.6 V, which should be expected, due to the increased bang gap for the ternary structure. The responsivity decreased to 0.07 A/W, possibly due to absorption in the ternary layer (η = 30%). These detectors were slow with a response speed of 1.6 μs, corresponding to a bandwidth of 100 kHz, and presented a NEP of 6.6×10^{-9} W. The dark current is attributed to both bulk leakage (dislocations and defects) and surface leakage (RIE damage to the perimeter) paths.

A tailoring of the band edge, in addition to an improvement in speed, were achieved by Monroy et al. [85] with the fabrication of a Schottky barrier detector on $Al_xGa_{1-x}N$:Si ($0 \le x \le 0.22$). The responsivity was independent of the Schottky contact (Au) size or diode size as well as incident power up to 2000 W/m^2. The wavelength cutoff shifted from 362 nm to 320 nm as the Al concentration increased from x = 0 to x = 0.22 with a visible rejection of > 10^3. The response speed improvement was strongest for the $Al_{0.22}Ga_{0.78}N$ detectors with response times as short as 14 ns. The 1/f limited detectors had a NEP of 16.3×10^{-9} W and 40.5×10^{-9} W, and detectivity of 6.1×10^9 and 1.2×10^9 cmHz$^{1/2}$/W, for GaN/Au and $Al_{0.22}Ga_{0.78}N$ detectors (at –2 V bias), respectively.

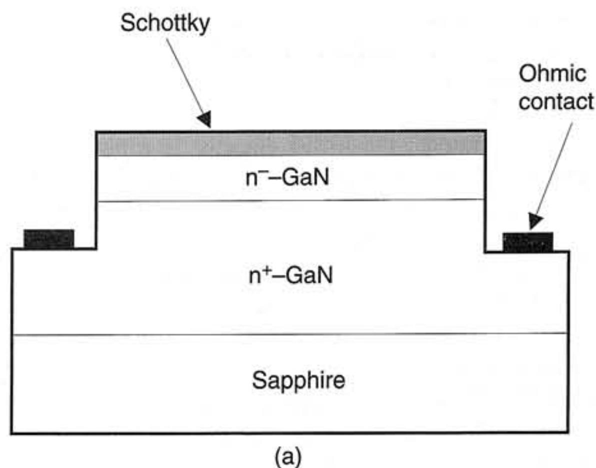

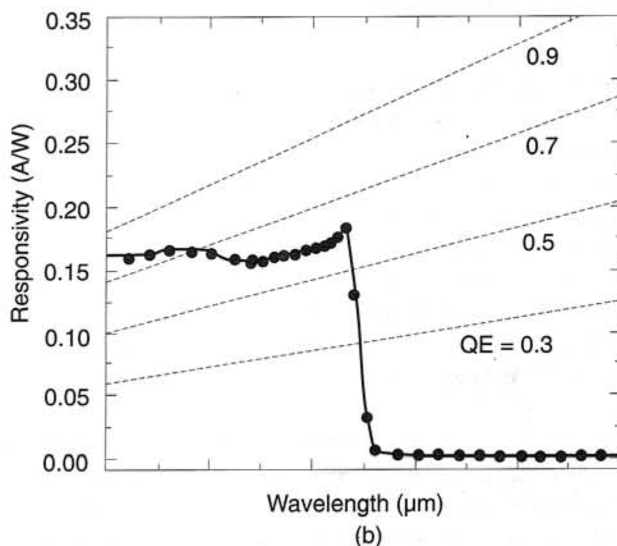

Fig. 7. Device structure (a) and spectral response (b) of a vertical Schottky detector under –5 V bias. A responsivity as high as 0.18 A/W was obtained (after Ref. 83).

To capitalise on well-developed handling and packaging methods, as well as the possibility of integrating nitride-based detectors with Si-based readout and control circuitry, investigations have been made of Schottky barrier detectors grown on Si (111). Also, since backside--illumination techniques are not as efficient for Schottky detectors, transparent (sapphire) substrates are not a necessity. Osinsky et al. [86] have reported on Pd/GaN Schottky barrier detectors grown on Si (111). These detectors turned on at 0.9 V, as expected, and had zero-bias responsivities of 0.05 A/W. They had a dark current of 1.5 μA/mm^2, and time response of ~70 ns (B = 2.2 MHz). The NEP, slightly lower than others mentioned in this section, was 3.7×10^{-9} W. At roughly 100 kHz, the 1/f noise was equal to that of the shot noise. Beyond that frequency the shot noise dominated.

A specific class of Schottky barrier photodetectors that has been receiving attention from the nitride community for the last couple of years is the Schottky metal-semiconductor-metal (MSM) photodiode. Similar to the Schottky barrier photodiode, the MSM detector is a planar device consisting of back-to-back Schottky contacts in an interdigitated pattern. An example of this pattern is shown in Fig. 8. The lateral transport design avoids electrical short-circuiting through threading dislocations that are so prevalent in GaN material. A large area of light absorption is provided by the interdigitated finger arrangement, while retaining small contact spacing to minimize transit time of the carriers. Dual Schottky barriers provide lower dark current than a Schottky diode alone, and the capacitance of a MSM diode is smaller than that of a p-i-n photodiode, which enhances the response speed. The MSM diode operates under a bias, which forward-biases one contact while reverse-biasing the other. Diagrams of the biased and unbiased energy band states are shown in Fig. 9.

At low biases, electron injection at the reverse-biased contact dominates the conduction mechanism. At higher biases, this conduction is supplemented by the injection of holes at the forward-biased contact. The depletion region at the reverse biased contact is much larger than the depleted region near the forward-biased contact, but when they meet the device is said to achieve the "reach through" condition. Although internal gain has been observed for these structures [5], it has not been fully understood and modeled.

Using Pt as the metal contacts, Carrano et al. [87] fabricated a GaN Schottky MSM detector with a low dark current of 22.8 nA/mm^2 at –10 V. The 1.5 μm thick, undoped GaN layer was grown by MOCVD. The responsivity was ~0.35 A/W at 350 nm, and the rejection of visible light was on the order of 10^2. The large responsivity indicated an internal gain mechanism, possibly hole trapping, although the gain was smaller than that found in a typical photoconductor. A later report [88] elucidated the transport mechanism present in this device, by comparing two MSM structures with different GaN thickness. The surface defects present in the thin GaN sample caused device degradation and transport dominated by a trap-assisted thermionic field emission process. The thicker GaN MSM device had carrier transport defined by thermionic emission with barrier lowering.

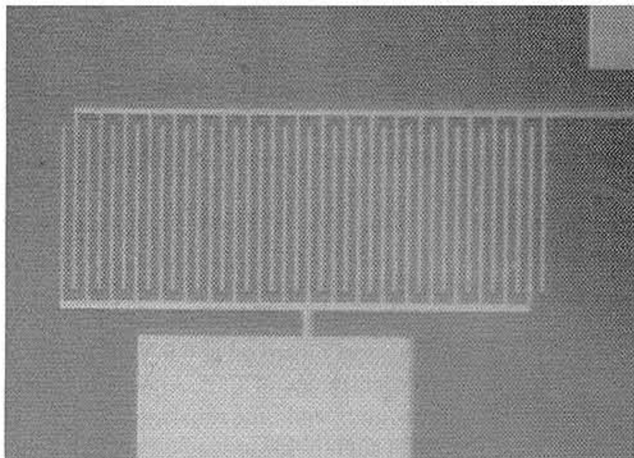

Fig. 8. Top view of MSM device showing interdigitated geometry. Finger width is 2 μm, length is 150 μm, and pitch is 10 μm.

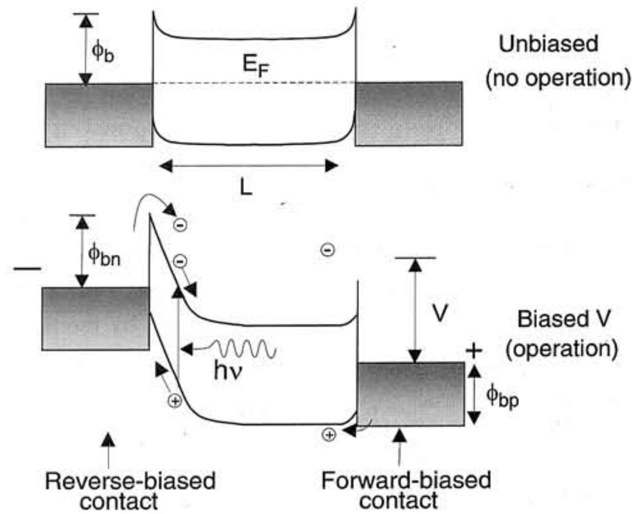

Fig. 9. The unbiased (non-operational) and biased (operational) energy band diagrams of a Schottky MSM photodetector.

Next, Carrano et al. [89] tested the characteristics of a MSM detector with an even thicker GaN layer (4 μm). This device gave a smaller dark current of ~32 nA/mm^2 and a responsivity of 0.15 A/W, showing no discernable internal gain. They characterized a "punch through" effect, which occurs in thinner GaN devices at high biases. This happened when the depletion region under the reverse bias electrode increased down to the nearly degenerate buffer layer, causing a sudden increase in dark current. In their last report on this topic to date, Carrano et al. [90] demonstrated a 10%-90% rise time for a Schottky MSM of ~23 ps, corresponding to a bandwidth of ~16 GHz, at 25 V. The devices were transit-time limited, for finger spacing (pitch) of 2 μm. A slow component of the decay was also observed and attributed to the slower hole drift velocity than the electron drift velocity.

The latest report by Walker et al. [91] on Schottky MSM detectors demonstrates low responsivities, indicative of an absence of internal gain, and a high visible rejection on the order of 10^5 for GaN and GaN:Mg based devices. Pt/Au metal layers were used as the Schottky contacts. Because the GaN and GaN:Mg layers were only ~1.2 μm thick, the lack of internal gain indicated high quality material. Time response measurements reported speeds of < 10 ns and 200 ns for the GaN and GaN:Mg MSM devices, respectively, and because the bias was only 1 V and the finger spacing 10 μm, the speeds and responsivities are not optimised. The dark currents were ~30 nA/mm^2 (GaN) and 200 nA/mm^2 (GaN:Mg) at 5 V bias. Noise information was also acquired for these devices. The 1/f-dominated noise power spectral density remained below the background level of the system, 10^{-24} A^2/Hz, up to 5 V for the

 © 2000 COSiW SEP, Warsaw

GaN:Mg MSM detector, and entirely below the background level for the GaN MSM detector.

6.3. Alternate photodiode schemes

One such problem that has been facing the nitride detector community has been the lack of internal gain in a reasonably fast detection scheme. As can be easily seen in the previous sections, p-n photodiodes often suffer from low responsivities and could therefore, not produce adequate signal levels for low light applications. Photoconductors typically have gain on the order of 10^3, yet are speed limited by the very mechanism which provides the photoconductive gain. Trapped charges in the photoconductors cause them to exhibit persistent photoconductivity as well as make them thermally unstable. Very limited success has been indicated in reports on avalanche photodiodes, a popular way to achieve a high gain configuration [92]. A high leakage current, probably due to high defect density, is incurred in GaN p-n junctions before they reach breakdown. These shortcomings of popular detection configurations lead to the analysis of other schemes that can be employed to detect UV radiation using GaN material.

Yang, *et al.* [93] recently reported on a high gain GaN/AlGaN heterojunction phototransistor. This device consisted of a sapphire substrate, AlN buffer layer, 1.7 μm n-$Al_{0.2}Ga_{0.8}N$ contact layer, 0.3 μm GaN collector, 0.2 μm p-GaN base, and a 0.5 μm n-GaN emitter, as shown in Fig. 10(a). Backside illumination lead to a build up of holes in the floating base, which lowered the p-GaN base barrier, increasing the electron injection from the emitter to provide gain. Although one would normally expect a slow recombination process to remove the holes in the base, this device can be biased to achieve punch through and force the holes into the emitter, thus resetting or "quenching" the detector quickly. This design cleverly circumvents the gain versus speed trade-off found in most detectors. A high responsivity of ~10^4 A/W existed in the band pass area between 320 nm and 360 nm. Clearly shown in Fig. 10(b), a rejection to visible light of 10^8 was also demonstrated. Despite the high gain in the UV region, the phototransistor exhibited extremely small photoresponse at 400 nm and above because the transition of electrons from donor states did not create carriers that could drift to the base and affect the barrier height. Also, the quenching process likely filled most gap states in the undoped region, making transitions from the valence bands to this state unlikely. The variable frequency of optical quenching permits tailoring of the gain/speed ratio for specific applications. This device appears to be very successful, but further work should be done to obtain noise response measurements.

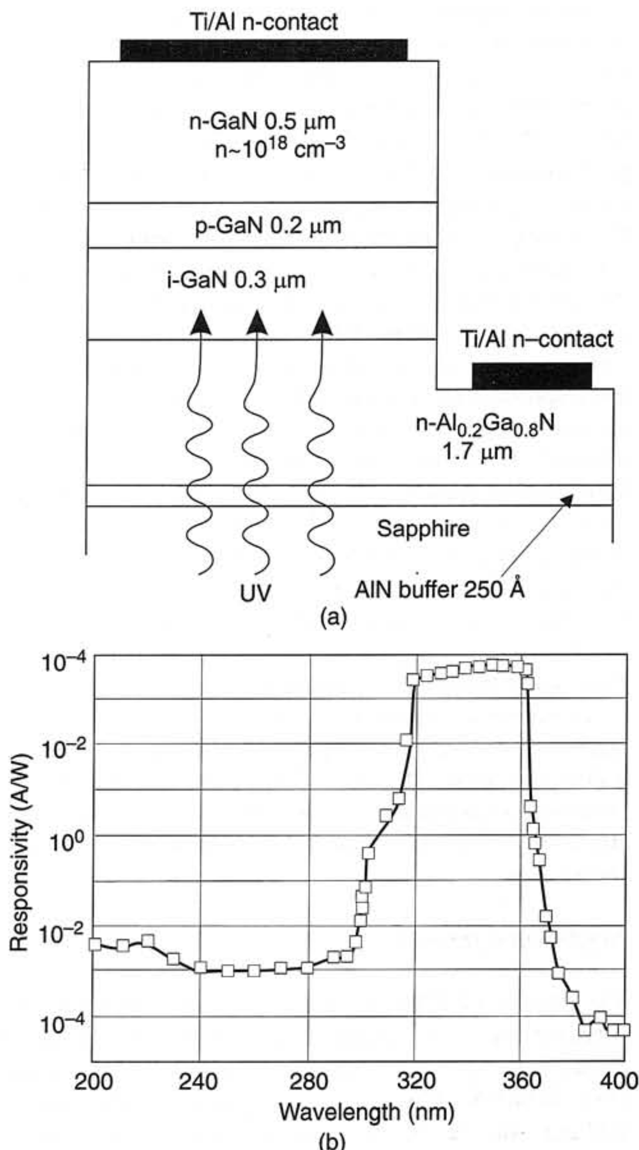

Fig. 10. Structure of the n-p-i-n GaN/AgaN heterojunction bipolar phototransistor (a), and spectral photoresponse (b) of the GaN/AlGaN phototransistor showing a sharp cutoff at 365 nm and eight orders of magnitude responsivity drop from 360 to 400 nm (after Ref. 93).

7. Conclusions

Advancements in UV photodetector technology are occurring at fast pace. Improved low resistance ohmic and high-quality Schottky contacts are being developed by incorporating semiconductor preparation and annealing techniques, in addition to an increased understanding of the mechanisms which dominate metal/GaN current transport. GaN etching (to form mesas) has been investigated by multiple groups. A variety of chemistries, chamber conditions and etching systems have been realized as a solution to the obstacles involved in etching such a resilient material. The investigation of defects and the roles they play as recombination centres, especially in contributing to PPC, was also outlined. Many similarities between defect behavior in GaN and the behaviour of DX states in AlGaAs were drawn. These led to the use of stretched exponential functions and lattice relaxation models to fit the PPC behaviour.

Recent reports of photoconductors with high gain, solar-blind p-n junction devices, and high speed Schottky barrier devices have been reviewed. Currently, photovoltaic devices such as p-i-n junctions and Schottky diodes are being researched most aggressively. The state of the art for photoconductors on GaN involve high responsivities, with a visible light rejection of about three orders of magnitude. The response speeds are slow due to the photoconductive gain. This gain has been found to decrease with increasing excitation power. P-n junction devices have been improved to offer high quantum efficiency (~80%), constant responsivity for a large excitation power range, and relatively fast response times (on the order of 10 ns). Advancements for p-n structures also include lower current leakage (67.5 pA/mm^2), higher rejection of visible light (10^6), and lower NEP. Recent work has demonstrated band edge tailoring using $Al_xGa_{1-x}N$ p-i-n structures. Due to the improvement of the Schottky barrier on GaN, Schottky barrier devices, including MSM designs, have been utilised to demonstrate very fast response times (~23 ps) at high bias. Devices based on the Schottky barrier have also demonstrated low noise and leakage current and high responsivity.

Applications involving low-light sources require a higher rejection of solar radiation than the typical GaN detectors mentioned here have been able to offer. Besides sensitivity improvements, band gap tailoring is an important issue that needs additional attention from the research community.

Acknowledgments

The authors would like to acknowledge the support and encouragement of M. Yoder, Y.S. Park, C. Wood, and J. Zolper from ONR, L. Lome from BMDO, and R. Leheny from DARPA. This work was partially supported by BMDO, and DARPA through ONR under contract N00014-93-1-0235 and N00014-99-1-0016.

References

1. M. Razeghi and A. Rogalski, *J. Appl. Phys.* **79**, 7433 (1996).
2. M.P. Ulmer, M. Razeghi, and E. Bigan, *Proc. SPIE.* **2397**, 210 (1995).
3. A. Rogalski and M. Razeghi, *Opto-Electr. Rev.* **4**, 13 (1996).
4. A. Rogalski, *Infrared Photon Detectors*, SPIE Optical Engineering Press, Bellingham, 1995.
5. P. Bhattacharya, *Semiconductor Optoelectronic Devices*, Prentice Hall, New Jersey, 1994.
6. J.S. Foresi and T.D. Moustakas, *Appl. Phys. Lett.* **62**, 2859 (1993).
7. S. Kurtin, T.C. McGill, and C.A. Mead, *Phys Rev. Lett.* **22**, 1433 (1969).
8. M.E. Lin, Z. Ma, F.Y. Huang, Z.F. Fan, L.H. Allen, and H. Morkoç, *Appl. Phys. Lett.* **64**, 1003 (1994).
9. D.W. Jenkins and J.D. Dow, *Phys. Rev.* **B39**, 3317 (1989).
10. Z. Fan, S.N. Mohammad, W. Kim, Ö. Aktas, A.E. Botchkarev, and H. Morkoç, *Appl. Phys. Lett.* 1692 (1996).
11. J.D. Guo, C.I. Lin, M.S. Feng, F.M. Pan, G.C. Chi, and C.T. Lee, *Appl. Phys. Lett.* **68**, 235 (1996).
12. S. Miller and P.H. Holloway, *J. Electr. Mater.* **25**, 1709 (1996).
13. S. Ruminov, Z. Liliental-Weber, J. Washburn, K.J. Duxstad, E.E. Haller, Z.F. Fan, S.N. Mohammad, W. Kim, A.E. Botchkarev, and H. Morkoç, *Appl. Phys. Lett.* **69**, 1556 (1996).
14. B.P. Luther, S.E. Mohney, T.N. Jackson, M.A. Khan, Q. Chen, and J.W. Yang, *Appl. Phys. Lett.* **70**, 57 (1997).
15. L.F. Lester, J.M. Brown, J.C. Ramer, L. Zhang, S.D. Hersee and J.C. Zolper, *Appl. Phys. Lett.* **69**, 2737 (1996).
16. J. Burm, K. Chu, W.A. Davis, W.J. Schaff, L.F. Eastman, and T.J. Eustis, *Appl. Phys. Lett.* **70**, 464 (1997).
17. Y.F. Wu, W.N. Jiang, B.P. Keller, S. Keller, D. Kapolnek, S.P. DenBaars, U.K. Mishra, and B. Wilson, *Solid State Electr.* **41**, 165 (1997).
18. C.T. Lee, M.Y. Yeh, C.D. Tsai, and Y.T. Lyu, *J. Electr. Mat.* **26**, 262, (1997).
19. A.T. Ping, M.A. Khan, and I. Adesida, *J. Electr. Mat.* **25**, 819, (1996).
20. T. Mori, T. Kozawa, T. Ohwaki, Y. Taga, S. Nagai, S. Yamasaki, S. Asami, N. Shibata, and M. Koite, *Appl. Phys. Lett.* **69**, 3537 (1996).
21. H. Ishekawa, S. Kobayashi, Y. Koide, S. Yamasaki, S. Nagai, J. Umezaki, M. Koike, and M. Murakami, *Appl. Phys. Lett.* **81**, 1315 (1997).
22. J.S. Jang, I.S. Chang, H.K. Kim, T.Y. Seong, S. Lee, and S.J. Park, *Appl. Phys. Lett.* **74**, 70 (1999).
23. M. Suzuki, T. Kawakami, T. Arai, S. Kobayashi, Y. Koide, T. Uemura, N. Shibata, and M. Murakami, *Appl. Phys. Lett.* **74**, 275 (1999).
24. J.K. Ho, C.S. Jong, C.C. Chiu, C.N. Huang, C.Y. Chen, and K.K. Shih, *Appl. Phys. Lett.* **74**, 1275 (1999).
25. E.H. Rhoderick and R.H. Williams, *Metal-Semiconductor Contacts*, Clarendon, Oxford, 1988.
26. A.S. Barker and M. Ilegems, *Phys. Rev.* **B7**, 743 (1973).
27. P. Blood, and J.W. Orton, *The Electrical Characterisation of Semiconductors: Majority Carriers and Electron States*, Academic Press, London, 1992.
28. J.D. Guo, M.S. Feng, R.J. Guo, F.M. Pan, and C.Y. Chang, *Appl. Phys. Lett.* **67**, 2657 (1995).
29. A.C. Schmitz, A.T. Ping, M.A. Khan, Q. Chen, J.W. Yang, and I. Adesida, *Semicond. Sci. Tchnol.* **11**, 1464 (1996).
30. L. Wang, M.I. Nathan, T.H. Lim, M.A. Khan, and Q. Chen, *Appl. Phys. Lett.* **68**, 1267 (1996).
31. E.V. Kalinina, N.I. Kuznetsov, V.A. Dmitriev, K.G. Irvine, and C.H. Carter, *J. Electr. Mat.* **25**, 831 (1996).
32. T.U. Kampen and W. Mönch, *MRS Internet J.* **1**, 41 (1997).
33. Q.Z. Liu, L.S. Yu, S.S. Lau, J.M. Redwing, N.R. Perkins, and T.F. Kuech, *Appl. Phys. Lett.* **70**, 1275 (1997).
34. J.K. Sheu, Y.K. Su, G.C. Chi, M.J. Jou, and C.M. Chang, *Appl. Phys. Lett.* **72**, 3317 (1998).
35. H.S. Venugopalan, S.E. Mohney, J.M. DeLucca, B.P. Luther, and G.E. Bulman, J. *Vac. Sci. Technol.* **A16**, 607 (1998).
36. K. Shiojima, T. Sugahara, and S. Sakai, *Appl. Phys. Lett.* **74**, 1936 (1999).
37. D. Walker, P. Kung, P. Sandvik, and M. Razeghi (unpublished).

 © 2000 COSiW SEP, Warsaw

38. M.T. Hirsch, K.J. Duxstad, and E.E. Haller, *Electr. Lett.* **33**, 95 (1997).
39. J.R. Mileham, S.J. Pearton, C.R. Bernathy, J.D. MacKenzie, R.J. Shul, and S.P. Kilcoyne, *J. Vac. Sci. Technol.* **A14**, 836 (1996).
40. C. Youtsey, I. Adesida, L.T. Romano, and G. Bulman, *Appl. Phys. Lett.* **72**, 560 (1998).
41. *Thin Film Processes II*, edited by J. Vossen and W. Kern, Academic Press, Boston, 1991.
42. F. Binet, J.Y. Buboz, N. Laurent, C. Bonnat, P. Collot, F. Hanauer, O. Briot, and R.L. Aulombard, *Appl. Phys. Lett.* **72**, 960 (1998).
43. R.J. Shul, S.P. Kilcoyne, M. Hagerott-Crawford, J.E. Parmeter, C.B. Vartuli, C.R. Abernathy, and S.J. Pearton, *Appl. Phys. Lett.* **66**, 1761 (1995).
44. C.B. Vartuli, S.J. Pearton, C.R. Abernathy, R.J. Shul, A.J. Howard, S.P. Kilcoyne, J.E. Parmeter, and M. Hagerott--Crawford, *J. Vac. Sci. Technol.* **A14**, 1011 (1996).
45. R.J. Shul, G.B. McCellan, S.A. Casalnouvo, D.J. Rieger, S.J. Pearton, C. Constantine, C. Barratt, R.F. Karlicek, C. Tran, and M. Schurman, *Appl. Phys, Lett.* **69**, 1119 (1996).
46. S.A. Smith, C.A. Wolden, M.D. Bremser, A.D. Hanser, R.F. Davis, and W.V. Lampert, *Appl. Phys. Lett.* **71**, 3631 (1997).
47. C.B. Vartuli, J.D. MacKenzie, J.W. Lee, C.R. Abernathy, S.J. Pearton, and R. Shul, *J. Appl. Phys.* **80**, 3705 (1996).
48. C.B. Vartuli, S.J. Pearton, C.R. Abernathy, R. J. Shul, A.J. Howard, S.P. Kilcoyne, J.E. Parmeter, and M. Hagerott--Crawford, *J. Vac. Sci. Tech.* A **14**, 1011 (1996).
49. J.Y. Lin, A. Dissanayake, G. Brown, and H.X. Jiang, *Phys. Rev.* **B42**, 5855 (1990).
50. C. Johnson, J.Y. Lin, H.X. Jiang, M.A. Khan, and C.J. Sun, *Appl. Phys. Lett.* **68**, 1808 (1996).
51. J.Z. Li, J.Y. Lin, H.X. Jiang, A. Salvador, A. Botchkarev, and H. Morkoç, *Appl. Phys. Lett.* **69**, 1474 (1996).
52. F. Binet, J.Y. Duboz, and E. Rosencher, F. Scholz, and V. Härle, *Appl. Phys. Lett.* **69**, 1202 (1996).
53. H.M. Chen, Y.F. Chen, M.C, Lee, and M.S. Feng, *Appl. Phys. Lett.* **82**, 899 (1997).
54. C.V. Reddy, K. Balakrishnan, H. Okumura, and S. Yoshida, *Appl. Phys. Lett.* **73**, 244 (1998).
55. M.T. Hirsch, J.A. Wolk, W. Walukiewicz, and E.E. Haller, *Appl. Phys. Lett.* **71**, 1098 (1997).
56. G. Beadie, W.S. Rabinovich, A.E. Wickenden, D.D. Koleske, S.C. Binari, and J.A. Freitas, *Appl. Phys. Lett.* **71**, 1092 (1997).
57. C.H. Qiu and J.I. Pankove, *Appl. Phys. Lett.* **70**, 1983 (1997).
58. X.Z. Dang, C.D. Wang, E.T. Yu, K.S. Boutros, and J.M. Redwing, *Appl. Phys. Lett.* **72**, 2745 (1998).
59. J.Z. Li, J.Y. Lin, H.X. Jiang, and M.A. Khan, *Appl. Phys. Lett.* **72**, 2868 (1998).
60. M.A. Khan, J.N. Kuznia, D.T. Olson, J.M. Van Hove, M. Blasingame, and L.F. Reitz, *Appl. Phys. Lett.* **60**, 2917 (1992).
61. M. Misra, T.D. Moustakas, R.P. Vaudo, R. Singh, and K.S. Shah, *Proc. SPIE* **2519**, 78 (1995).
62. K.S. Stevens, M. Kinniburgh, and R. Beresford, *Appl, Phys. Lett.* **66**, 3518 (1995).
63. C.H. Qiu, C. Hoggatt, W. Melton, M.W. Leksono, and J.I. Pankove, *Appl. Phys. Lett.* **66**, 2712 (1995).
64. P. Kung, X. Zhang, D. Walker, A. Saxler, J. Piotrowski, A. Rogalski, and M. Razeghi, *Appl. Phys. Lett.* **67**, 3792 (1995).
65. F. Binet, J.Y. Duboz, E. Rosencher, F. Scholz, and V. Härle, *Appl. Phys. Lett.* **69**, 1202 (1996).
66. D. Walker X. Zhang, P. Kung, A. Saxler, S. Javadpour, J. Xu, and M. Razeghi, *Appl. Phys. Lett.* **68**, 2100 (1996).
67. D. Walker, P. Kung, A. Saxler, P. Kung, J. Xu, and M. Razeghi, *Appl. Phys. Lett.* **70**, 949 (1997).
68. E. Muñoz, E. Monroy, J.A. Garrido, I. Izpura, F.J. Sánchez, M.A. Sánchez-García, E. Calleja, B. Beaumont, and P. Gibart, *Appl. Phys. Lett.* **71**, 870 (1997).
69. X. Zhang, P. Kung, D. Walker, J. Pietrowski, A. Rogalski, A. Saxler, and M. Razeghi, *Appl. Phys. Lett.* **67**, 2028 (1995).
70. F. Binet, J.Y. Buboz, N. Laurent, E. Rosencher, O. Briot, and R.L. Aulombard, *J. Appl. Phys.* **81**, 6449 (1997).
71. Q. Chen, M.A. Khan, C.J. Sun, and J.W. Yang, *Electronic Letters* **31**, 1781 (1995).
72. J.M. Van Hove, R. Hickman, J.J. Klassen, P.P. Chow, and P.P. Ruden, *Appl. Phys. Lett.* **70**, 2282 (1997).
73. G.Y. Xu, A. Salvador, W. Kim, Z. Fan, C. Lu, H. Tang, H. Morkoç, G. Smith, M. Estes, B. Goldenberg, W. Yang, and S. Krishnankutty, *Appl. Phys. Lett.* **71**, 2154 (1997).
74. A. Osinsky, S. Gangopadhyay, R. Gaska, B. Williams, M.A. Khan, D. Kuksenkov, and H. Temkin, *Appl. Phys. Lett.* **71**, 2334 (1997).
75. P. Kozodoy, J.P. Ibbetson, H. Marchand, P.T. Fini, S. Keller, J.S. Speck, S.P. DenBaars, and U.K Mishra, *Appl. Phys. Lett.* **73**, 975 (1998).
76. D. Walker, A. Saxler, P. Kung, X. Zhang, M. Hamilton, J. Diaz, and M. Razeghi, *Appl. Phys. Lett.* **72**, 3303 (1998).
77. S. Krishnankutty, W. Yang, A.T. Nohava, and P. Ruden, *MRS Internet J. of Nitride Semiconductor Research* **3**, 7 (1998).
78. E. Monroy, E. Muñoz, F.J. Sánchez, F. Calle, E. Calleja, B. Beaumont, P. Gibart, J.A. Muñoz, and F. Cussó, *Semicond. Sci. Technol.* **13**, 1 (1998).
79. E. Monroy, M. Hamilton, D. Walker, P. Kung, F.J. Sánchez, and M. Razeghi, *Appl. Phys. Lett.* **74**, 1171 (1999).
80. P. Schreiber, T. Dang, G. Smith, T. Pickenpaugh, P. Gehred, and C. Litton, *Proc. SPIE* **3629**, 184 (1999).
81. D. Walker, P. Kung, P. Sandvik, J. Wu, M. Hamilton, I.H. Lee, J. Diaz, and M. Razeghi, *Proc. SPIE* **3629**, 193 (1999).
82. M.A. Khan, J.N. Kuznia, D.T. Olson, M. Blasingame, and A.R. Bhattarai, *Appl. Phys. Lett.* **63**, 2455 (1993).
83. Q. Chen, J.W. Yang, A. Osinsky, S. Gangopadhyay, B. Lim, M.Z. Anwar, M.A. Khan, D. Kuksenkov, and H. Temkin, *Appl. Phys. Lett.* **70**, 2277 (1997).
84. A. Osinsky, S. Gangopadhyay, B.W. Lim, M.Z. Anwar, M.A. Khan, D.V. Kuksenkov, and H. Temkin, *Appl. Phys. Lett.* **72**, 742 (1998).
85. E. Monroy, F. Calle, E. Muñoz, F. Omnés, P. Gibart, and J.A. Muñoz, *Appl. Phys. Lett.* **73**, 2146 (1998).
86. A. Osinsky, S. Gangopadhyay, J.W. Yang, R. Gaska, D. Kuksenkov, H. Temkin, I.K. Shmagin, Y.C. Chang, J.F. Muth, and R.M. Kolbas, *Appl. Phys. Lett.* **72**, 551 (1998).
87. J.C. Carrano, P.A. Grudowski, C.J. Eiting, R.D. Dupuis, and J.C. Campbell, *Appl. Phys. Lett.* **70**, 1992 (1997).
88. J.C. Carrano, T. Li, P.A. Grudowski, C.J. Eiting, R.D. Dupuis, and J.C. Campbell, *Appl. Phys. Lett.* **72**, 542 (1998).

89. J.C. Carrano, T. Li, P.A. Grudowski, C.J. Eiting, R.D. Dupuis, and J.C. Campbell, *J. Appl. Phys*. **83**, 6148 (1998).
90. J.C. Carrano, T. Li, D.L. Brown, P.A. Grudowski, C.J. Eiting, R.D. Dupuis, and J.C. Campbell, *Appl. Phys. Lett.* **73**, 2405 (1998).
91. D. Walker, E. Moñroy, P. Kung, J. Wu, M. Hamilton, F.J. Sanchéz, J. Diaz, and M. Razeghi, *Appl. Phys. Lett.* **74**, 762 (1999).
92. V.A. Dmitriev, K.G. Irvine, C.H. Carter, N.I. Kuznetsov, and A.V. Kalinina, *Appl. Phys. Lett.* **68**, 229 (1996).
93. W. Yang, T. Nohava, S. Krishnankutty, R. Torreano, S. McPherson, and H. Marsh, *Appl. Phys. Lett.* **73**, 978 (1998).

 © 2000 COSiW SEP, Warsaw